Hindawi
Advances in Civil Engineering
Volume 2019, Article ID 8041767, 10 pages
https://doi.org/10.1155/2019/8041767

Research Article

Shear Lag Effects in Angles Welded at Both Legs

Mohammad Abedin,[1] **Shervin Maleki**,[2] **Nafiseh Kiani**,[3] **and Esmail Shahrokhinasab**[1]

[1]*Department of Civil and Environmental Engineering, Florida International University, Miami, FL, USA*
[2]*Department of Civil Engineering, Sharif University of Technology, Tehran, Iran*
[3]*Department of Civil, Architectural and Environmental Engineering, University of Miami, Coral Gables, FL, USA*

Correspondence should be addressed to Mohammad Abedin; mabed005@fiu.edu

Received 4 April 2019; Accepted 5 September 2019; Published 22 September 2019

Academic Editor: Abdul Aziz bin Abdul Samad

The shear lag phenomenon is known to reduce the tensile capacity of tension members. There are various parameters affecting shear lag that have not been considered before. In addition, previous studies have been conducted mainly on single steel sections. Using numerical methods, the present study investigates the effects of relevant parameters on shear lag in single- and double-angle sections welded at both legs. The studied parameters are connection eccentricity, connection length, gusset plate thickness, member-free length, and connection-free length. The results of the numerical analyses show that, in single-angle connections, the effects of connection length, connection eccentricity, and gusset plate thickness are more pronounced, while in double-angle connections the last parameter is not very critical. Comparing the results with the AISC-LRFD predictions, it is concluded that the specification relations are conservative in most cases. In order to reduce the overconservatism, some new equations for shear lag estimate are introduced.

1. Introduction

In steel structures, sections such as angles, channels, and hollow sections, among others, are generally used as tension members in bracings and truss configurations. As such, only part of the cross section is usually connected to the gusset plate, which causes nonuniform distribution of stresses in the tension member near the connecting element (Figure 1). In addition, the line of action of the load usually does not coincide with the centroidal axis of a tension member, and hence, eccentric loading and bending of the member is induced. The combination of these effects leads to the shear lag phenomenon and possible member rupture in the connection area. In this phenomenon, various parameters, such as connection eccentricity, connection length, and gusset plate thickness, have been proven to play a role. Design specifications consider the impact of this phenomenon as a reduction factor applied to the area of the cross section. However, ways and approaches in determining this factor vary in different specifications. The common equation given in AISC [1] specification to calculate the shear lag factor of tension members is as follows:

$$U = \frac{1 - \overline{x}}{l}, \tag{1}$$

where U is the shear lag coefficient, which is equal to unity for a connection that ensures uniform stress distribution over the section; $\overline{x}$ is the distance from the shear plane to the center of gravity of the tension member; and l is the length of connection.

The basis of this equation is the studies and experiments conducted by Munse and Chesson [2, 3] on bolted and riveted connections, which has been verified by comparing the results of more than 1000 tests. Since then, numerous studies on shear lag in tension members with different cross sections have been conducted. Gibson and Wake [4] conducted experiments on single- and double-angle sections with balanced and unbalanced weld connections. They showed that, in single angles, the use of balanced welds increases the member's strength. Easterling and Gonzalez

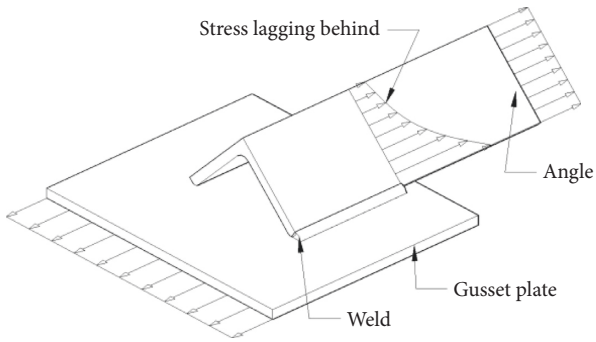

Figure 1: Shear lag in single angle.

[5] examined the basis of the AISC equations by testing more than 27 specimens with welded connections. They recommended that the upper limit for the shear lag coefficient should be 0.9. In a study by Barth et al. [6], tension behavior of WT sections with bolted connections was investigated. One of the aims of their research was to investigate the bending effects caused by eccentricity of loading. Humphries and Birkemoe [7] showed that the equations presented in the Canadian steel standard for the shear lag were generally conservative. Zhu et al. [8] conducted 13 angle tests with welded connections. Based on the test results, both the ultimate loads sustained by the short leg connected angles and the ductility of all the angle specimens were greater when the balanced weld arrangement was used in the connections. Also, Teh et al. [9–13] executed numerical and experimental tests on many bolted sections to determine the shear lag effects. Xiong et al. [14] conducted a limited numerical study of shear lag of high-strength steel bolted and welded angles.

As was pointed out, there have been numerous studies in recent years to investigate the effect of shear lag on tension members with welded and bolted connections; however, the effects of some effective parameters on this phenomenon, such as member symmetry and gusset plate thickness, have not been studied. Member symmetry occurs in double-angle or channel connections. Furthermore, the arrangement of single and double angles as shown in Figure 2 has not been investigated before. Therefore, design specifications provide no particular equation whatsoever for these conditions. Note that, for welded angles, this arrangement provides a higher radius of gyration and resistance to buckling than back-to-back angles.

This paper aims at studying numerically the effective parameters influencing shear lag in single- and double-angle sections arranged as shown in Figure 2. Specifically, the effects of connection length (L_W), gusset plate thickness (t_G), member-free length (L), and gusset plate-free length (L_G) on angles with different sizes are considered (see Figure 2 for parameter definitions).

2. Finite Element Model

The finite element (FE) models of single- and double-angle members are created in the environment of ABAQUS [15] software. Three-dimensional 8-node brick elements (C3D8RH) with hybrid formulation and the reduced integration method are used for all steel members [16]. Both material and geometric nonlinearities are considered in the models. Because of the symmetry of the model and to reduce the computational costs, a one-eighth model for double angles and a one-quarter model for single angles are used. In the symmetry planes, appropriate symmetrical boundary conditions are applied. In order to simulate the loading, a uniform linear displacement load has been applied to the end of the gusset plate to obtain displacement-based plastic deformations. The ultimate load of each model is obtained on the force-displacement diagram of the member and is called P_{FEM}. The shear lag coefficient is calculated from equation (2). In this equation, F_U is the ultimate strength of steel material and A_g is the gross area of the section:

$$U = \frac{P_{FEM}}{F_U A_g}. \tag{2}$$

Properties of the steel and weld materials are based on Guo's [17] tension test. The steel is CSA G40.21-M grade 300W, and welding is performed with E48018 electrodes. The material model is considered as isotropic with elastic-plastic hardening. For simulation of materials in the software, the true stress and strain values have been calculated using the following equations:

$$\begin{aligned} \sigma_{true} &= \sigma_{nom}\left(1 + \varepsilon_{nom}\right), \\ \varepsilon^{pl}_{true} &= Ln\left(1 + \varepsilon_{nom}\right) - \left(\frac{\sigma_{true}}{E}\right), \end{aligned} \tag{3}$$

where σ_{true} is the true stress, σ_{nom} is the nominal stress, ε_{nom} is the nominal strain, and ε^{pl}_{true} is the true plastic strain.

By converting the engineering stress-strain into true stress-strain and extrapolation by the use of power law, the true stress-strain diagram for steel and weld metal is obtained, as shown in Figure 3. The ductile damage fracture criterion of ABAQUS has been used for more accurate modeling of the materials and better observation of the specimen's fracture location in the finite element model [18, 19]. Figure 4 illustrates a typical FE model of a tension member with tensile fracture at the critical section.

2.1. Fracture Initiation. The ductile damage initiation criterion available in ABAQUS is a model for predicting damage in ductile members such as steel. The model assumes that the equivalent plastic strain at the onset of damage ($\bar{\varepsilon}^{pl}_0$) is a function of stress triaxiality (η) and strain rate, as shown below:

$$\begin{aligned} \bar{\varepsilon}^{pl}_0 &= \bar{\varepsilon}^{pl}_0(\eta), \\ \eta &= \frac{\sigma_m}{\bar{\sigma}}, \end{aligned} \tag{4}$$

where

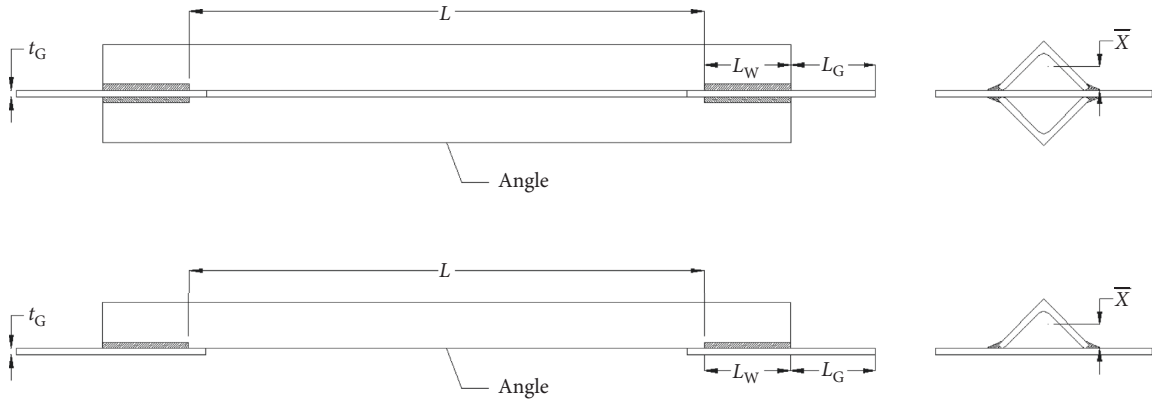

Figure 2: Single- and double-angle tension members.

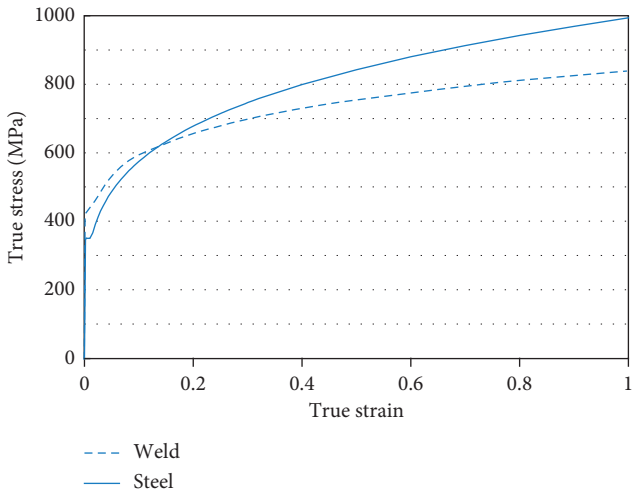

Figure 3: True stress-strain for steel material.

$$\sigma_m = \frac{(\sigma_1 + \sigma_2 + \sigma_3)}{3},$$
$$\overline{\sigma} = \sqrt{\frac{\left[(\sigma_1 - \sigma_2)^2 + (\sigma_2 - \sigma_3)^2 + (\sigma_3 - \sigma_1)^2\right]}{2}}. \quad (5)$$

Fracture or damage is assumed to initiate when the equivalent plastic strain ($\overline{\varepsilon}^{pl}$) reaches ($\overline{\varepsilon}_0^{pl}$). The relation of stress triaxiality with the equivalent plastic strain at the onset of damage can be expressed as [20]

$$\overline{\varepsilon}_0^{pl} = \begin{cases} \infty, & \eta \le -\dfrac{1}{3}, \\ \dfrac{C_1}{1 + 3\eta}, & -\dfrac{1}{3} \le \eta \le 0, \\ C_1 + (C_2 - C_1)\left(\dfrac{\eta}{\eta_0}\right)^2, & 0 \le \eta \le \eta_0, \\ \dfrac{C_2\eta_0}{\eta}, & \eta_0 \le \eta, \end{cases} \quad (6)$$

where C_2 and C_1 are the plastic strains at failure under uniaxial tension ($\eta = 1/3$) and pure shear ($\eta = 0$), respectively. C_2 can be calculated from the reduction in area (A_R) of a uniaxial axisymmetric tensile specimen as follows:

$$C_2 = -\ln(1 - A_R). \quad (7)$$

To calculate the C_1 coefficient, the following equation can be used:

$$C_1 = C_2\left(\frac{\sqrt{3}}{2}\right)^{1/m}. \quad (8)$$

The parameter m is obtained by considering the true stress-strain exponential relation of the material or the power law, $\sigma = K\varepsilon^m$. Furthermore, $\eta_0 = 1/3$ is a good approximation of the stress triaxiality at the center of the specimen [21].

2.2. Fracture Evolution. Figure 5 illustrates the characteristic stress-strain behavior of a material undergoing damage. In the context of an elastic-plastic material with isotropic hardening, the damage manifests itself in two forms: softening of the yield stress and degradation of elasticity. The solid curve in Figure 5 represents the damaged true stress-strain response, while the dashed curve is the response in the absence of damage. The damaged response depends on the element dimensions such that mesh dependency of the results is minimized and damaged elements reaching the ductile damage criterion (DUCTCRT) of 1 are eliminated from the models automatically.

As was pointed out, in order to model the fracture of ductile materials, certain parameters, such as material ductility C_2 and equivalent plastic displacement $\overline{u}^{pl}$, need to be calculated based on the standard coupon tension test. In order to determine these parameters, Guo's tension coupon tests were modeled and values of the material ductility C_2 of 0.2 and the plastic displacement at failure $\overline{u}^{pl}$ equal to 6 mm were found to be compatible with the test results after several iterations.

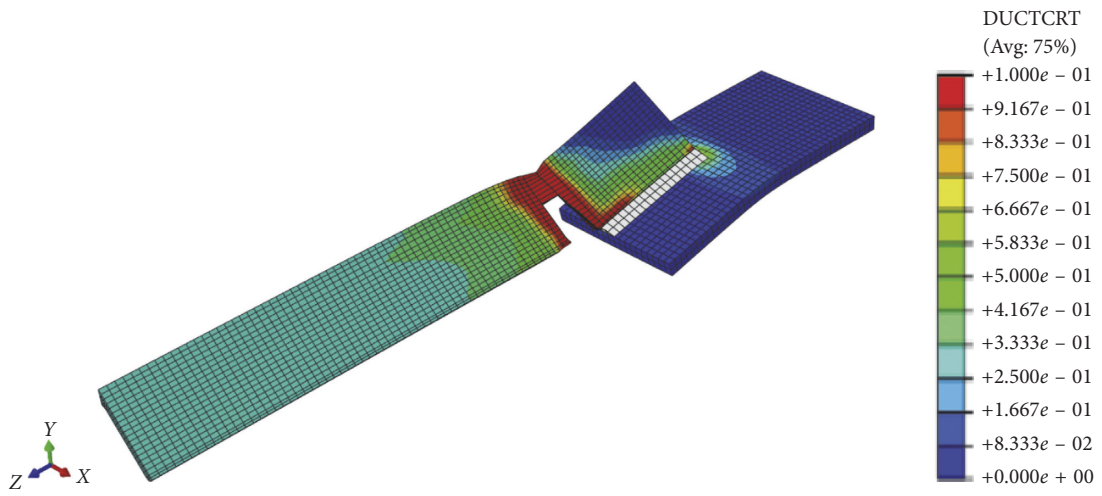

Figure 4: FE model showing fracture at the critical section.

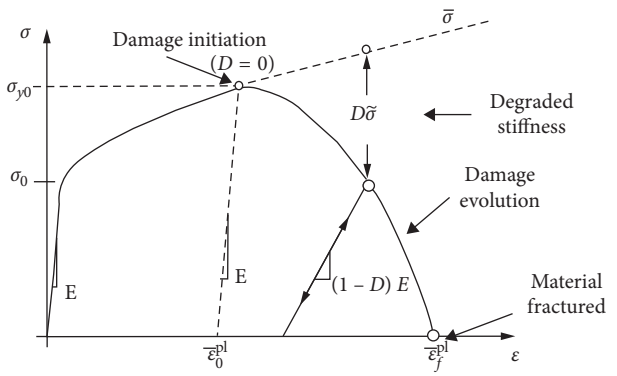

Figure 5: Stress-strain curve with progressive damage degradation, ABAQUS [15].

3. Verification of the FE Model

Guo's experimental results on channel tension members have been used to assess the accuracy of the steel stress-strain relationship, the damage criterion, and other modeling assumptions. In Guo's experimental results, only four of the ten specimens failed by fracture of the gross section and the other six specimens had weld failure. To this end, the four specimens that had fracture in the gross section of the member were modeled in ABAQUS with the assumptions explained in the previous sections. All the models used C75 × 6 channel sections with back-to-back welded connections to the gusset. Table 1 gives the details of the specimens along with experimental and numerical results. As is clear, the results of the numerical analyses are within 4% of the experimental results. In addition, the area of fracture, like the test, has also occurred in the gross section away from the critical area, as is shown in Figure 6, and the failure mode was correctly predicted in all specimens. Furthermore, in order to evaluate the tension behavior of the specimens with experimental results, the force-displacement diagram has been studied for every specimen, and it was observed that the tensile behavior of the specimens is compatible with the experimental behavior. Figure 7 shows the load-deflection curve obtained from the test and FE model for specimen 1.

4. Parametric Analysis

The calibrated FE model is used for parametric analyses on angle tension members. The properties of angles used are shown in Table 2. In order to see the effects of each parameter on the shear lag of tension members, that particular parameter was varied while other parameters were held constant. The results of numerical analyses are discussed and plotted for each parameter in the subsequent sections.

4.1. Connection Length. Figures 8 and 9 show the results obtained from numerical models with various connection lengths for single and double angles, respectively. As seen in the figures, increasing the connection length (L_W) increases the shear lag coefficient towards 1. This means there is less shear lag in the member. Tension force which is transmitted to the gusset plate through welding will be distributed throughout the length of the weld and thus leads to a more uniform distribution of stress. This in turn reduces stress concentration at the toe of the critical section and increases the tension capacity of the member (Figure 10). The results show that the relation between the connection length and the shear lag coefficient is linear up to a certain point (optimum connection length) which stress distribution is almost uniform over the connection length and there is significantly less improvement in the stress distribution and shear lag coefficient beyond this point. The effect of the connection length on the single angle is far more than on the double angles, in a way that an increase of 25% in length of the weld on the average leads to an increase of 10% in tension capacity in single angles and 4.5% in double angles.

Table 1: Comparison of the analysis results with experimental results of Guo.

Specimen	Single/double channel	Welding detail	Weld size (mm)	Weld length (mm)	Test failure mode	FEM failure mode	Ultimate load (kN)		P_{Test}/P_{FEM}
							Test	FEM	
1	Double	Longitudinal	5	115	GF	GF	750	759	0.99
2	Double	Longitudinal	10	60	GF	GF	730	760	0.96
8	Single	Longitudinal	5	100	GF	GF	369	378	0.98
9	Double	Longitudinal	5	100	GF	GF	742	760	0.98

GF = gross section fracture.

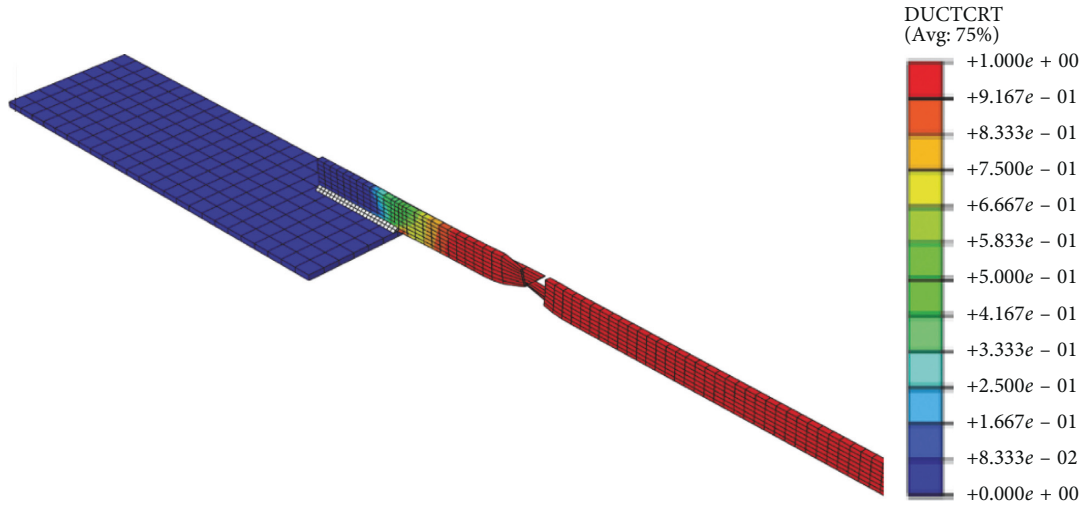

Figure 6: Fracture of specimen 1 in the FE model.

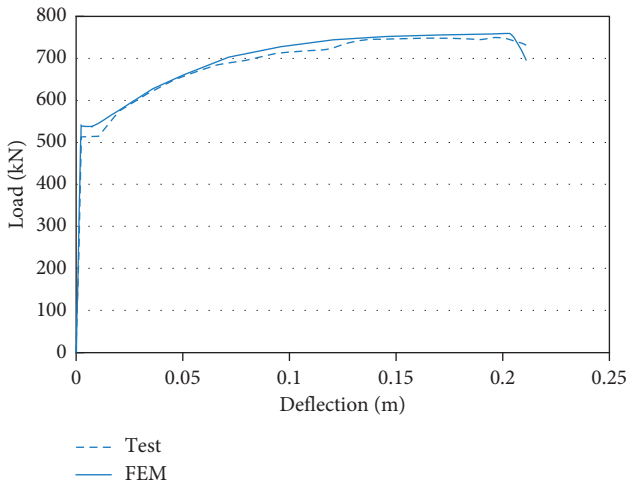

Figure 7: Comparison of load- deflection curves obtained from the test and FE model for specimen 1.

4.2. Gusset Plate Thickness. According to Figure 11, the increase in the gusset plate thickness (t_G) in single angles results in the bending stiffness increase; therefore, the gusset plate shows more resistance against the moment resulted from eccentricity and will face less bending deformation. The stress concentration is reduced at the toe of the critical section and distributed more uniformly over the connection length, and as a result, the tension capacity of the member is increased.

Table 2: Details of angle sections.

Angle	a (mm)	s (mm)	r_1 (mm)	r_2 (mm)	A (mm^2)	$\overline{x}$ (mm)
L100 × 10	100	10	12	6	1920	35.4
L120 × 12	120	12	13	6.5	2750	42.6
L150 × 15	150	15	16	8	4300	53.3
L200 × 16	200	16	18	9	6180	70.9

a = leg length; s = thickness; r_1 = root radius; r_2 = toe radius; A = area of section; $\overline{x}$ = distance from the shear plane to the center of gravity.

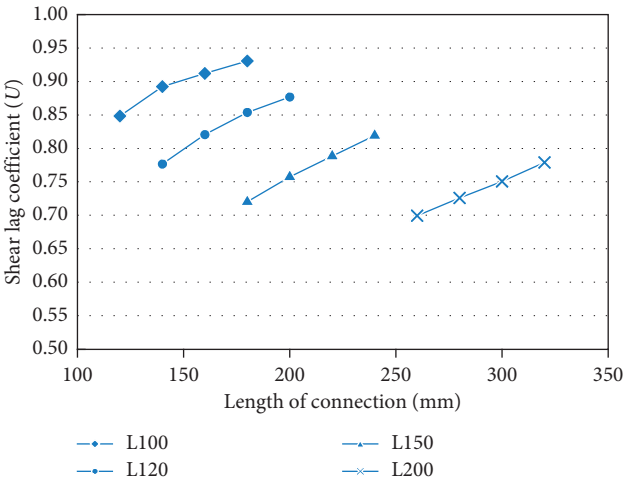

Figure 8: Effect of connection length on the tension capacity of single angles.

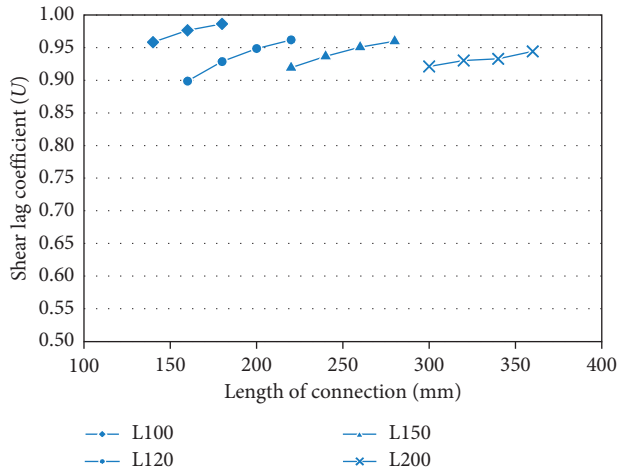

Figure 9: Effect of connection length on the tension capacity of double angles.

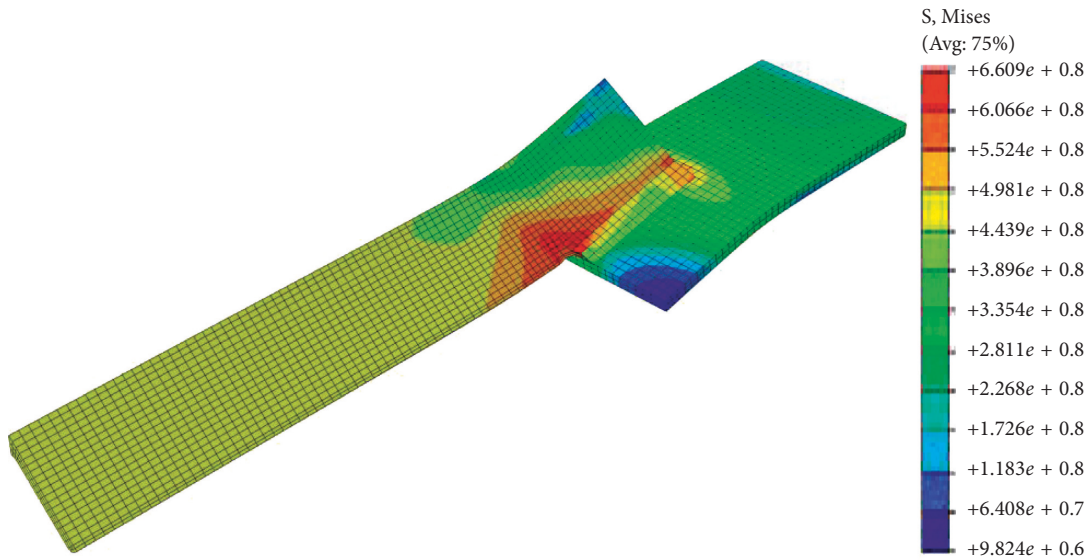

Figure 10: Stress distribution for single-angle connections.

As shown in Figure 12, the effect of this parameter is quite different in double angles. In double-angle connections, because of symmetry, bending moments caused by eccentricity on the two sides cancel each other and there is no significant moment in the gusset plate. Therefore, the increase or decrease of the gusset plate thickness neither affects the bending deformation of the gusset plate nor the tension capacity of double angles.

It should be noted that the width of the gusset plate in the specimens is considered more than the Whitmore width (30 degrees extension on the two sides) so as to distribute the stresses throughout the plate. Gusset plate thickness in the specimens varied from 10 mm to 30 mm. There were a number of models in which the low gusset plate thickness has resulted in excessive bending in the plate, which ultimately, as shown in Figure 13, has led to the rupture in the gusset plate. This mode of failure is not the subject of this study.

4.3. Member-Free Length. To study the effects of the member-free length (L), several models were examined. The rule for naming models is that the size of the angle is mentioned first, followed by the connection length (L_W), then weld size, gusset plate thickness (t_G), and the configuration of the angles (being single or double, noted as s or d). According to Figure 14, it can be concluded that the member-free length does not have much effect on the tension capacity of single and double angles.

4.4. Gusset Plate-Free Length. To investigate the effect of gusset plate-free length, several models were examined. In all models, the member-free length was kept at 1200 mm. As shown in Figure 4, all models experience gusset plate bending along the connection length to some extent. However, no significant bending deformation is seen in the area of the gusset plate-free length. Thus, increasing or decreasing the

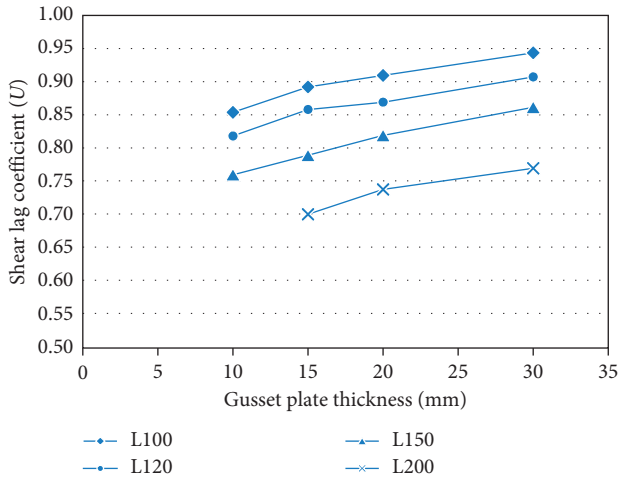

Figure 11: Effect of gusset plate thickness on the tension capacity of single angles.

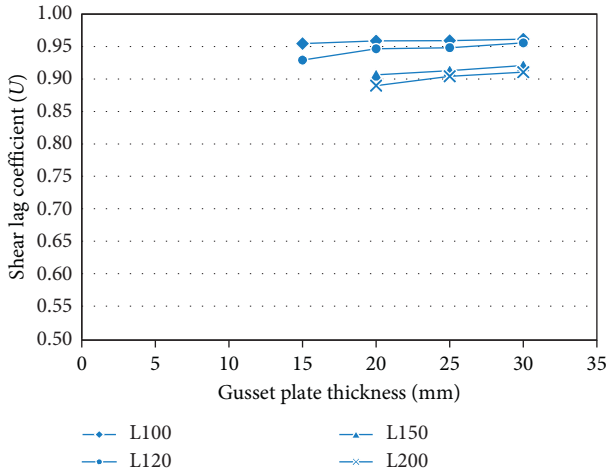

Figure 12: Effect of gusset plate thickness on the tension capacity of double angles.

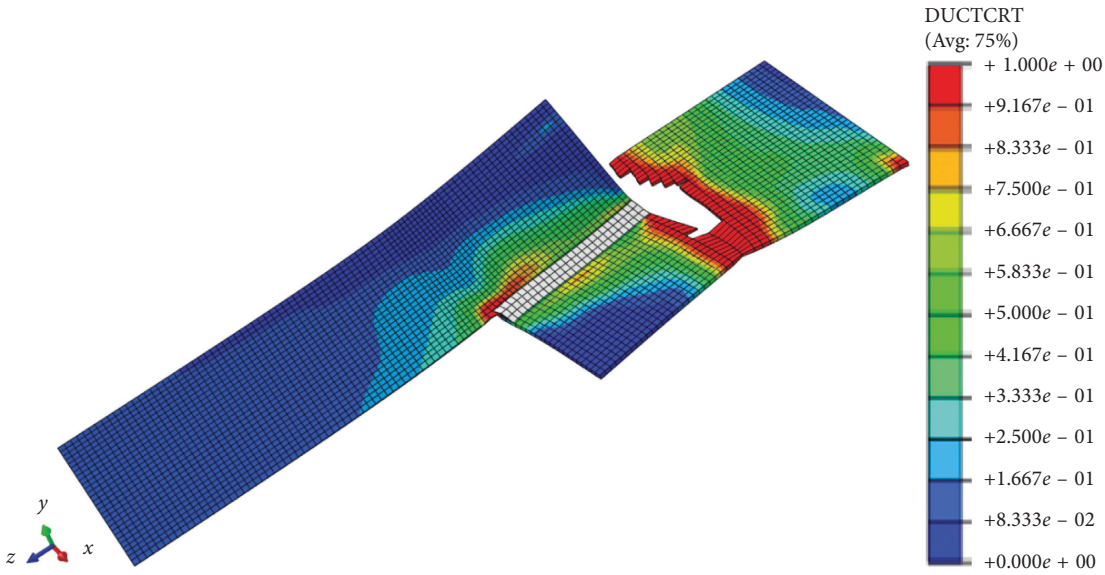

Figure 13: The rupture of the gusset plate in the finite element model.

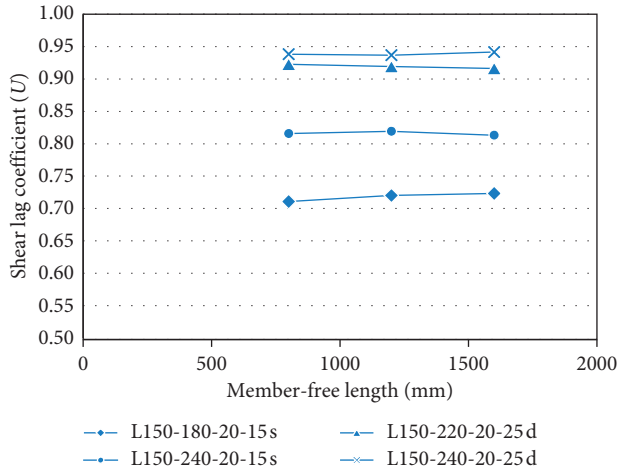

Figure 14: Effect of member-free length on the tension capacity of single and double angles.

Table 3: Comparison of the results of numerical analyses with the AISC equation.

Model	Section	L_W (mm)	Weld size (mm)	t_G (mm)	Failure mode	Ultimate load (kN)	F_uA_g (kN)	U_{AISC}	U_{FEM}	U_{FEM}/U_{AISC}
L100-120-10-15s	L100	120	10	15	NF	894.1	1053.9	0.71	0.85	1.20
L100-140-10-15s		140	10	15	NF	940.3		0.75	0.89	1.19
L100-160-10-15s		160	10	15	NF	961.2		0.78	0.91	1.17
L100-180-10-15s		180	10	15	NF	980.5		0.8	0.93	1.16
L100-120-10-20d	L100	120	10	20	SR	1879.5	2107.8	–	–	–
L100-140-10-20d		140	10	20	NF	2019.5		0.75	0.96	1.28
L100-160-10-20d		160	10	20	NF	2058.3		0.78	0.98	1.26
L100-180-10-20d		180	10	20	NF	2078.6		0.8	0.99	1.24
L120-180-12-10s	L120	180	12	10	NF	1244	1521	0.76	0.82	1.08
L120-180-12-15s		180	12	15	NF	1304.9		0.76	0.86	1.13
L120-180-12-20s		180	12	20	NF	1321.7		0.76	0.87	1.14
L120-180-12-30s		180	12	30	NF	1379.7		0.76	0.91	1.2
L150-220-18-15d	L150	220	18	15	GPF	3565.6	4754	–	–	–
L150-220-18-20d		220	18	20	NF	4308.4		0.76	0.91	1.2
L150-220-18-25d		220	18	25	NF	4339.6		0.76	0.91	1.2
L150-220-18-30d		220	18	30	NF	4377		0.76	0.92	1.21
L200-260-20-15s	L200	260	20	15	NF	2389.6	3416.5	0.73	0.7	0.96
L200-280-20-15s		280	20	15	NF	2480		0.75	0.73	0.97
L200-300-20-15s		300	20	15	NF	2564.5		0.76	0.75	0.99
L200-320-20-15s		320	20	15	NF	2661.3		0.78	0.78	1

NF = net section fracture; GPF = gusset plate fracture; SR = shear rupture; s/d = single or double angles.

free length has no effect on bending deformation of the connection area and stress concentration at the toe of the critical section. Hence, the gusset plate-free length has no effect on the tension capacity of single and double angles.

5. AISC Shear Lag Equation

The equation in AISC specification for calculating the shear lag coefficient (equation (1)) only considers the effects of two parameters: eccentricity and the connection length. The shortcoming of this equation could be the lack of an appropriate factor to calculate the shear lag coefficient in double angles (or channels). To calculate this coefficient in double-angle connections, one must consider each angle separately and thus use the proposed equation for single sections, which seems to be conservative.

Considering the numerical analyses results, the equation of the AISC specification for single angles of ordinary size (L100 and L120) seems to be conservative. However, the equation for angles with large sizes, such as L200, is nonconservative. Moreover, in the AISC equation, the effect of gusset plate thickness on tension capacity of the member has not been considered. Also, for double angles, by not considering the symmetry, the AISC equation becomes overly conservative. Table 3 summarizes the results of some selected numerical analyses and compares them with the AISC shear lag factor. The last column shows the ratio of the shear lag factor obtained by the two methods. Obviously, for

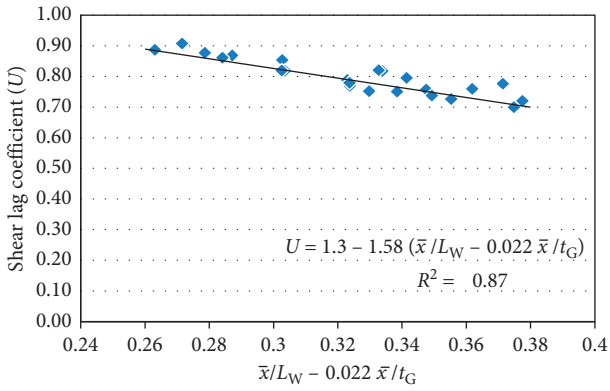

Figure 15: Proposed equation for the single angle compared to FE results.

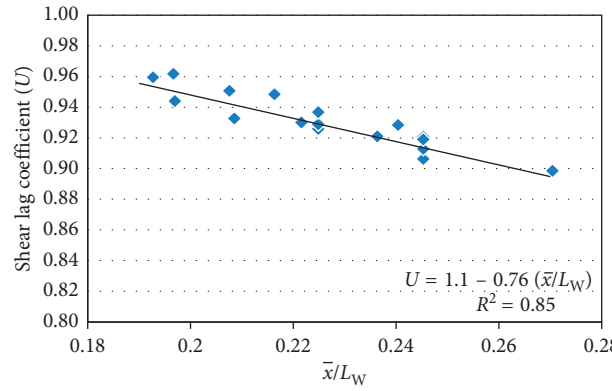

Figure 16: Proposed equation for the double angle compared to FE results.

double angles, there is up to 28% conservatism in the AISC equation.

Therefore, by providing a new equation for single- and double-angle connections, one can correct this equation to better match the obtained results as follows.

5.1. Single Angles. Among various parameters, the parameters $\bar{x}$, L_W, and t_G have been chosen as the most effective parameters to be incorporated in the revised equation. Having U_{FEM} obtained from the finite element analyses of the specimens, the best curve fit using the three effective parameters in various states resulted in the following equation:

$$U = 1.3 - \frac{1.58\bar{x}}{L_W} - \frac{0.03\bar{x}}{t_G} \leq 1. \quad (9)$$

5.2. Double Angles. In double-angle connections, the parameters L_W and $\bar{x}$ are more critical, while the parameter t_G does not have much effect. Therefore, for simplicity and for the sake of similarity to the equation of the specification, we consider the parameter $\bar{x}/L_W$ as the effective parameter; and the following equation is the best curve fit for the calculation of the coefficient of the shear lag in double angles:

$$U = 1.1 - \frac{0.76\bar{x}}{L_W} \leq 1. \quad (10)$$

Figures 15 and 16 show the error of the proposed equations compared to FE results.

6. Conclusions

In this paper, using finite element analyses, the shear lag phenomenon and tension behavior of single- and double-angle sections with welded connections at both legs were investigated. The parameters considered are connection eccentricity, connection length, gusset plate thickness, member-free length, and gusset plate-free length. The FE models were calibrated against the existing test results. The ductile damage criterion was used in the models to accurately predict failure patterns.

Considering the results of finite element analyses, it is concluded that, in single-angle connections, other than the well-known connection eccentricity and length, the gusset plate thickness also plays an important role. With an increase in the gusset plate thickness, the bending stiffness also increases, and therefore, the gusset plate will show much more resistance against the moment caused by eccentricity. Hence, stress concentration decreases at the toe of the critical section and distributes more uniformly over the connection length, and as a result, the tensile capacity of the angle increases.

In double-angle connections, only the two parameters of connection eccentricity and length are important, while the gusset plate thickness, due to symmetry of loading and vanishing gusset bending stresses, has no effect. In addition, other parameters such as the gusset plate-free length and the member-free length were found to be trivial in both single- and double-angle connection shear lags.

Although the AISC specification neglects the effect of the gusset plate thickness in its suggested shear lag equation, it can conservatively predict the tension capacity of single-angle tension members. However, this equation in double-angle connections is overly conservative (up to 28% in cases considered), and this is due to the lack of consideration of symmetry. Therefore, to better predict the shear lag in single and double angles with lesser conservatism, the following equations are suggested:

$$U = 1.3 - \frac{1.58\bar{x}}{L_W} - \frac{0.03\bar{x}}{t_G} \leq 1, \quad \text{for single angles,}$$

$$U = 1.1 - \frac{0.76\bar{x}}{L_W} \leq 1, \quad \text{for double angles,} \quad (11)$$

where $\bar{x}$ is the connection eccentricity (mm), L_W is the connection length (mm), and t_G is the gusset plate thickness (mm).

Data Availability

The data supporting the findings of this study are available within the article.

Conflicts of Interest

The authors declare that they have no conflicts of interest.

References

[1] AISC ANSI/AISC 360-16, *Specification for Structural Steel Buildings*, American Institute of Steel Construction, Chicago, IL, USA, 2016.

[2] W. H. Munse and E. Chesson Jr, "Riveted and bolted joints: net section design," *Journal of the Structural Division (ASCE)*, vol. 89, pp. 107–126, 1963.

[3] E. Chesson Jr and W. H. Munse, "Riveted and bolted joints: truss-type tensile connections," *Journal of the Structural Division (ASCE)*, vol. 89, no. 5, pp. 329-330, 1963.

[4] G. J. Gibson and B. T. Wake, "An investigation of welded connections for angle tension members," *Journal of the American Welding Society*, vol. 7, p. 44, 1942.

[5] W. S. Easterling and L. G. Giroux, "Shear lag effects in steel tension members," *Engineering Journal*, vol. 30, pp. 77–89, 1993.

[6] K. E. Barth, J. G. Orbison, and R. Nukala, "Behavior of steel tension members subjected to uniaxial loading," *Journal of Constructional Steel Research*, vol. 58, no. 5–8, pp. 1103–1120, 2002.

[7] M. J. R. Humphries and P. C. Birkemoe, "Shear lag effects in fillet-welded tension connections of channels and similar shapes," in *Proceedings of the ECCS/AISC Workshop on Connections in Steel Structures V: Innovative Steel Connections*, pp. 381–392, Amsterdam, The Netherlands, June 2004.

[8] H. T. Zhu, M. C. H. Yam, A. C. C. Lam, and V. P. Iu, "The shear lag effects on welded steel single angle tension members," *Journal of Constructional Steel Research*, vol. 65, no. 5, pp. 1171–1186, 2009.

[9] L. H. Teh and V. Yazici, "Shear lag and eccentricity effects of bolted connections in cold-formed steel sections," *Engineering Structures*, vol. 52, pp. 536–544, 2013.

[10] L. H. Teh and M. E. Uz, "Block shear failure planes of bolted connections—direct experimental verifications," *Journal of Constructional Steel Research*, vol. 111, pp. 70–74, 2015.

[11] L. H. Teh and B. P. Gilbert, "Net section tension capacity of equal angle braces bolted at different legs," *Journal of Structural Engineering*, vol. 140, no. 6, Article ID 06014002, 2014.

[12] L. H. Teh and B. P. Gilbert, "Net section tension capacity of cold-reduced sheet steel channel braces bolted at the web," *Journal of Structural Engineering*, vol. 139, no. 5, pp. 740–747, 2013.

[13] L. H. Teh and B. P. Gilbert, "Net section tension capacity of cold-reduced sheet steel angle braces bolted at one leg," *Journal of Structural Engineering*, vol. 139, no. 3, pp. 328–337, 2013.

[14] Y. H. Xiong, A. C. C. Lam, M. C. H. Yam, and K. F. Chung, "Numerical study of shear lag of high strength steel bolted and welded angles," *Advances in Structural Engineering and Mechanics*, 2015.

[15] Dassault ABAQUS Documentation, *ABAQUS/CAE Doc*, Simulia, Providence, RI, USA, 2016.

[16] A. Ghaffary and R. Karami Mohammadi, "Framework for virtual hybrid simulation of TADAS frames using opensees and abaqus," *Journal of Vibration and Control*, vol. 24, no. 11, pp. 2165–2179, 2018.

[17] H. Guo, *Shear Lag Effect on Welded Hot-Rolled Steel Channel in Tension*, University of Alberta, Edmonton, Canada, 2005.

[18] M. Abedin, S. Farhangdoust, and A. B. Mehrabi, "Fracture detection in steel girder bridges using self-powered wireless sensors," in *Proceedings of the In Risk-Based Bridge Engineering: Proceedings of the 10th New York City Bridge Conference*, p. 216, CRC Press, New York, NY, USA, August 2019.

[19] M. Abedin and A. B. Mehrabi, "Novel approaches for fracture detection in steel girder bridges," *Infrastructures*, vol. 4, no. 3, p. 42, 2019.

[20] Y.-W. Lee and T. Wierzbicki, "Quick fracture calibration for industrial use," Impact Crashworthiness Lab Report, Massachusetts Institute of Technology, Cambridge, MA, USA, 2004.

[21] Y. Bao and T. Wierzbicki, "On fracture locus in the equivalent strain and stress triaxiality space," *International Journal of Mechanical Sciences*, vol. 46, no. 1, pp. 81–98, 2004.